Interferometric Spectroscopy of Scattered Light Can Quantify the Statistics of Subdiffractional Refractive-Index Fluctuations

L. Cherkezyan, I. Capoglu, H. Subramanian, J. D. Rogers, D. Damania, A. Taflove, and V. Backman*

Northwestern University, Evanston, Illinois 60208, USA

(Received 12 February 2013; published 19 July 2013)

Despite major importance in physics, biology, and other sciences, the optical sensing of nanoscale structures in the far zone remains an open problem due to the fundamental diffraction limit of resolution. We establish that the expected value of spectral variance ($\tilde{\Sigma}^2$) of a far-field, diffraction-limited microscope image can quantify the refractive-index fluctuations of a label-free, weakly scattering sample at subdiffraction length scales. We report the general expression of $\tilde{\Sigma}$ for an arbitrary refractive-index distribution. For an exponential refractive-index spatial correlation, we obtain a closed-form solution of $\tilde{\Sigma}$ that is in excellent agreement with three-dimensional finite-difference time-domain solutions of Maxwell's equations. Sensing complex inhomogeneous media at the nanoscale can benefit fields from material science to medical diagnostics.

DOI: 10.1103/PhysRevLett.111.033903 PACS numbers: 42.25.Dd, 42.25.Fx, 42.25.Hz, 87.64.−t

Do Maxwell's equations permit determining the nature of three-dimensional (3-D) subdiffractional refractive-index (RI) fluctuations of a linear, label-free dielectric medium in the far zone? Recently, by capturing high spatial-frequency evanescent waves, metamaterial-based lenses and grating-assisted tomography have achieved a resolving power no longer limited by the diffraction of light [1,2]. However, this super-resolution is confined to the transverse plane, which limits its ability to characterize 3-D inhomogeneous media.

Whereas various nonlinear techniques have been proposed to image subdiffractional structures in 3-D [3–5], these techniques require exogenous labeling or intrinsic fluorescence and, thus, only image the spatial distribution of particular molecular species.

Currently, elastic, label-free spectroscopic microscopy techniques are emerging that characterize the endogenous properties of a medium by utilizing the spectral content of a diffraction-limited microscopic image. Examples include multiple high-precision quantitative phase microscopy techniques [6–8], which measure the longitudinal integral of RI and, hence, are insensitive to longitudinal RI fluctuations. Alternatively, partial-wave spectroscopic microscopy [9], confocal light scattering and absorption spectroscopy [10], and spectral encoding of spatial frequency [11] analyze the light-scattering response of inhomogeneous materials to obtain information of their subdiffractional structure in both lateral and longitudinal dimensions. However, the reported theory behind these techniques involves strong assumptions such as one-dimensional light transport, approximation of the medium as solid spheres, or having a single length scale.

Here, we establish that the spectral signature of scattered light in a far-zone microscope image contains sufficient information to quantify the 3-D RI fluctuations of weakly scattering media at deeply subdiffractional scales. We report three-dimensional light transport theory for linear, label-free weakly scattering media with an arbitrary form of RI distribution: continuous or discrete, random or deterministic, statistically isotropic or not. We consider the expected value of spectral variance ($\tilde{\Sigma}^2$) of a far-field, diffraction-limited image registered by a microscope with a small numerical aperture (NA) of illumination and spectrally resolved image acquisition. We show that $\tilde{\Sigma}$ quantifies RI fluctuations at nanometer length scales limited only by the signal-to-noise ratio of the system. Under the single scattering approximation, we obtain an explicit expression relating $\tilde{\Sigma}$ to the statistics of RI fluctuations inside the sample. Moreover, for the special case of an exponential form of the RI spatial correlation, we present a closed-form solution for $\tilde{\Sigma}$ and validate it via numerical simulations of an experiment based on rigorous 3-D finite-difference time-domain (FDTD) solutions of Maxwell's equations [12].

Consider a spatially varying RI object sandwiched between two semi-infinite homogeneous media (Fig. 1). The RIs of the three media are, from top to bottom: n_0, $n_1[1 + n_\Delta(\mathbf{r})]$ (as a function of location $\mathbf{r}$), and n_2. To

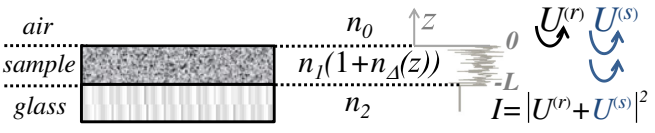

FIG. 1 (color online). Sample: RI of the middle layer is random, and RIs of the top and bottom layers are constant; RI as a function of depth is shown in gray. The coherent sum of $U^{(r)}$ and $U^{(s)}$ is detected. Reflection from the bottom of the substrate (glass slide) is negligible, as its thickness (1 mm) is much larger than the microscope's depth of field (for most setups, 0.5–15 μm).

begin with, we assume $n_1 = n_2$, approximating the case of fixed biological media on a glass slide [13,14].

A unit amplitude plane wave with a wave vector $\mathbf{k_i}$ is incident normally onto a weakly scattering sample. Under the Born approximation, the field inside the sample is uniform and has an amplitude $T_{01} = 2n_0/(n_0 + n_1)$ (transmission Fresnel coefficient). In the far zone, the scattering amplitude of the scalar field $U^{(s)}$, scattered from the RI fluctuations $n_\Delta(\mathbf{r})$ in the direction specified by the wave vector $\mathbf{k_o}$, is $f_s(\mathbf{k_s}) = T_{01}\int(k^2/2\pi)n_\Delta(\mathbf{r}')e^{-i\mathbf{k_s}\cdot\mathbf{r}'}d^3\mathbf{r}'$, where $\mathbf{k_s} = \mathbf{k_o} - \mathbf{k_i}$ is the scattering wave vector (inside the sample) [15]. The scalar-wave approximation is used here as it sufficiently describes the intensity image formed by a microscope with a moderate NA [15]. Its further justification by full-vector 3-D FDTD results is discussed below.

When the sample is imaged by an epi-illumination bright-field microscope, the back-propagating field reflected from the sample's top surface, $U^{(r)}$, returns to the image plane. Meanwhile, only the part of $U^{(s)}$ that propagates at solid angles within the NA of the objective is collected. For a microscope with magnification M, moderate NA ($k_z \approx k$), ignoring the angular dependence of the Fresnel coefficient $T_{10} = 2n_1/(n_0 + n_1)$, $U^{(s)}$ focused at a point (x', y') in the image plane is [16]

$$U^{(s)}_{\mathrm{im}}(x', y', k) = \frac{kT_{10}}{i2\pi|M|}\iint T_{k\mathrm{NA}} f_s e^{-i(k_x x' + k_y y')} d\frac{k_x}{k} d\frac{k_y}{k}, \tag{1}$$

where $T_{k\mathrm{NA}}$ is the microscope's pupil function—a cone in the spatial-frequency space with a radius kNA [Fig. 2(a)]. Thus, the objective performs low-pass transverse-plane spatial frequency filtering, with the cutoff corresponding to the spatial coherence length. With substitution of f_s into Eq. (1) and the introduction of a windowing function $T_{\mathbf{k_s}}$ that equals 1 at $\mathbf{k} = \mathbf{k_s}$ and 0 at $\mathbf{k} \neq \mathbf{k_s}$ [Fig. 2(a)], $U^{(s)}_{\mathrm{im}}$ is

$$U^{(s)}_{\mathrm{im}}(x', y', k) = \frac{T_{10}T_{01}}{i|M|}\int_{-\infty}^{\infty} k n_{1\mathrm{D}}(\mathbf{r}) e^{-i2kz} dz, \tag{2}$$

where $\mathbf{r}$ is $(x'/M, y'/M, z)$ inside the sample, and $n_{1\mathrm{D}}$ is the $n_\Delta(\mathbf{r})$ convolved ($\otimes$) with the unitary Fourier transform

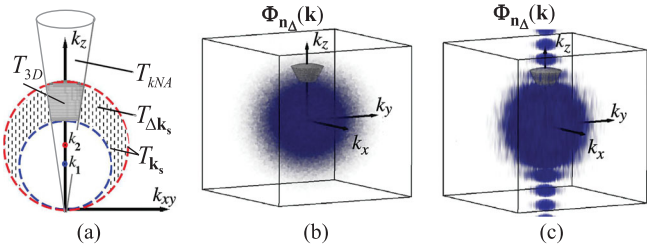

FIG. 2 (color). Spatial-frequency space with k_z axis antiparallel to $\mathbf{k_i}$. (a) Cross section of $T_{\Delta\mathbf{k_s}}$, $T_{k\mathrm{NA}}$, and their interception $T_{3\mathrm{D}}$; (b) PSD of the RI fluctuation (blue) and $T_{3\mathrm{D}}$ (gray) when $l_c \ll L$ and (c) $l_c \lesssim L$.

($\mathcal{F}$) of $T_{k\mathrm{NA}}T_{\mathbf{k_s}}$ in the transverse plane (xy, $\perp$), $n_{1\mathrm{D}}(\mathbf{r}) = \mathcal{F}_\perp\{T_{k\mathrm{NA}}T_{\mathbf{k_s}}\} \otimes_\perp n_\Delta(\mathbf{r})$.

Equation (2) presents a new treatment of the Born approximation, which is here extended to include the optical imaging of a scattering object in the far zone. Mathematically, Eq. (2) signifies that to describe a microscope-generated spectrum (a 1-D signal), the 3-D problem of light propagation can be reduced to a 1-D problem where the RI is convolved with the Airy disk in the transverse plane.

The microscope image intensity (normalized by the image of the source) is an interferogram

$$I(x', y', k) = \Gamma_{01}^2 - 2\Gamma\,\mathrm{Im}\left\{\int_{-\infty}^{+\infty} k n_{1\mathrm{D}}(\mathbf{r}) e^{-i2kz} dz\right\}, \tag{3}$$

where $\Gamma_{01} = (n_0 - n_1)/(n_0 + n_1)$ is the Fresnel reflectance coefficient, $\Gamma = \Gamma_{01}T_{01}T_{10}$, Im denotes "the imaginary part of," and $n_{1\mathrm{D}}$ is zero at $z \notin (-L, 0)$. Here, $O(n_\Delta^2)$ terms are neglected.

We quantify the spatial distribution of n_Δ via Σ^2, the spectral variance of the image intensity within the illumination bandwidth Δk. Since the expectation of the spectrally averaged image intensity equals Γ_{01}^2, $\Sigma^2(x', y')$ is defined as $\Sigma^2(x', y') = \int_{\Delta k}(I(x', y', k) - \Gamma_{01}^2)^2 dk/\Delta k$. For convenience, we introduce a windowing function $T_{\mathbf{\Delta k_s}}$ that is a unity at $\mathbf{k} = \mathbf{k_s}$ for all $\mathbf{k_i}$ with magnitudes within the Δk of the system and is zero elsewhere [$|\mathbf{k_i}|$ between k_1 and k_2 in Fig. 2(a)]. On denoting k_c as the value of the central wave number of illumination bandwidth inside the sample, approximation of $\Delta k \ll k_c$, and application of the convolution and the Parseval's theorems [for mathematical details see the Supplemental Material [17]], $\Sigma^2(x', y')$ equals

$$\Sigma^2(x', y') = \frac{\Gamma^2 k_c^2}{\Delta k}\int_{-\infty}^{\infty} |\mathcal{F}\{T_{\Delta\mathbf{k_s}}T_{k\mathrm{NA}}\} \otimes n_\Delta(\mathbf{r})|^2 dz. \tag{4}$$

Physically, $T_{\mathbf{\Delta k_s}}$ accounts for the limited bandwidth of illumination and serves as a bandpass longitudinal spatial-frequency filter of RI distribution with its width related to the temporal coherence length $l_\tau = 2\pi/\Delta k$. The interception of the two frequency filters associated with the spatial and temporal coherence, $T_{k\mathrm{NA}}$ and $T_{\mathbf{\Delta k_s}}$, signifies the frequency-space coherence volume centered at $k_z = 2k_c$: $T_{3\mathrm{D}} = T_{\mathbf{\Delta k_s}}T_{k\mathrm{NA}}$ [Fig. 2(a)]. Given an infinite bandwidth, one could reconstruct the full 3-D RI from $I(x', y', k)$. However, since Δk and k_c are finite, Σ detects the variance of an "effective RI distribution," i.e., of $n_\Delta(\mathbf{r}) \otimes \mathcal{F}\{T_{3\mathrm{D}}\}$ [Eq. (4)].

Note that $\Sigma^2(x', y')$ is random since $n_\Delta(\mathbf{r})$ is random. Hence, to characterize the sample statistics, we compute its expected value, denoted as $\tilde{\Sigma}^2$. Using the Wiener-Khinchine relation, we obtain $\tilde{\Sigma}^2$ from Eq. (4) as

$$\tilde{\tilde{\Sigma}}^2 = \frac{\Gamma^2 k_c^2 L}{\Delta k} \int_{T_{3D}} \mathbf{\Phi}_{\mathbf{n}_\Delta}(\mathbf{k}) d^3\mathbf{k}, \quad (5)$$

where $\mathbf{\Phi}_{\mathbf{n}_\Delta} = |\mathcal{F}\{\mathbf{n}_\Delta(\mathbf{r})\}|^2$ is the power spectral density (PSD) of n_Δ.

Equation (5) establishes the general quadrature-form expression for $\tilde{\tilde{\Sigma}}^2$ for an arbitrary $n_\Delta(\mathbf{r})$. Note that while the 3-D structure of complex inhomogeneous materials cannot be described by a single measure of size or RI, the PSD fully quantifies the magnitude, spatial frequency, and orientation of all RI fluctuations present within the sample. As seen from Eq. (5), $\tilde{\tilde{\Sigma}}^2$ measures the integral of the tail of the PSD within T_{3D}. Hence, as shown later, $\tilde{\tilde{\Sigma}}^2$ presents a monotonic measure of the width of the PSD. When $n_1 \neq n_2$, the expression for $\tilde{\tilde{\Sigma}}^2$ has a different prefactor and a deterministic offset, specified in the Supplemental Material [17].

We further obtain a closed-form expression for $\tilde{\tilde{\Sigma}}^2$ for a special case when $n_\Delta(\mathbf{r})$ has an exponential form of spatial correlation with a variance σ_{n_Δ} and correlation distance l_c. Since l_c can only be defined for a random medium with a physical size much larger than the correlation distance, we define l_c as the correlation distance of an unbounded medium $n_\Delta^\infty(\mathbf{r})$ and the sample as a horizontal slice of $n_\Delta^\infty(\mathbf{r})$ with thickness L: $n_\Delta(\mathbf{r}) = T_L n_\Delta^\infty(\mathbf{r})$ where T_L is a windowing function along the z axis with width L. The PSD of such sample is an anisotropic function of l_c and L: $\mathbf{\Phi}_{\mathbf{n}_\Delta}(\mathbf{k}) = |\mathcal{F}\{T_L\} \otimes \mathcal{F}\{n_\Delta^\infty\}|^2$ [Figs. 2(b) and 2(c)]. Alternatively, $\tilde{\tilde{\Sigma}}^2$ is found by independently computing the contributions from (i) scattering from within the sample ($\tilde{\tilde{\Sigma}}_R^2$) and (ii) reflectance at $z = -L$ ($\tilde{\tilde{\Sigma}}_L^2$),

$$\tilde{\tilde{\Sigma}}^2 = \tilde{\tilde{\Sigma}}_R^2 + \tilde{\tilde{\Sigma}}_L^2. \quad (6)$$

Here, $\tilde{\tilde{\Sigma}}_L$ is fully described by the RI contrast at the bottom surface $\tilde{\tilde{\Sigma}}_L^2 = \Gamma^2 \sigma_\perp^2(n_{1D})/4$, where $\sigma_\perp^2(n_{1D})$ is the variance of the effective n_{1D} in the transverse plane [details shown in the Supplemental Material [17]]. $\tilde{\tilde{\Sigma}}_R$, in turn, is defined by $\mathbf{\Phi}_{\mathbf{n}_\Delta^\infty}$, which is independent of L when $L \gtrsim l_\tau$; $\tilde{\tilde{\Sigma}}_R^2$ is obtained by integrating the PSD of an exponentially correlated $n_\Delta^\infty(\mathbf{r})$ according to Eq. (5). Substituting $\tilde{\tilde{\Sigma}}_R^2$ and $\tilde{\tilde{\Sigma}}_L^2$ into Eq. (6) and introducing a unitless size parameter $x = k_c l_c$, we obtain the following closed-form solution for $\tilde{\tilde{\Sigma}}^2$ for an exponential form of the spatial RI correlation:

$$\tilde{\tilde{\Sigma}}^2 = \frac{2\Gamma^2 \sigma_{n_\Delta}^2}{\pi} \frac{k_c L x^3 \mathrm{NA}^2}{[1 + x^2(4 + \mathrm{NA}^2)](1 + 4x^2)} + \Gamma^2 \sigma_{n_\Delta}^2 [1 - 1/\sqrt{1 + (x\mathrm{NA})^2}]/4. \quad (7)$$

Two assumptions were made to derive Eq. (7) from Eq. (5): (1) we approximated the top and bottom surfaces of T_{3D} as planes perpendicular to the k_z axis, and (2) we calculated $\tilde{\tilde{\Sigma}}_R$ from $\mathbf{\Phi}_{\mathbf{n}_\Delta^\infty}$, not considering the extreme case of $L \ll l_\tau$. Both assumptions are not crucial from the theoretical perspective and are there only to obtain a relatively simple closed-form solution of Eq. (5).

To confirm these approximations, we evaluate $\tilde{\tilde{\Sigma}}$ predicted by the general quadrature-form expression [Eq. (5)] using MATLAB computing software (MathWorks Inc.). We obtain an excellent agreement between $\tilde{\tilde{\Sigma}}$ calculated from Eq. (5) and the closed-form expression [Eq. (7)] derived from it (Fig. 3). This validates the closed-form solution for $\tilde{\tilde{\Sigma}}$ for an exponential RI correlation.

We support the present theory by simulating a physical experiment using the rigorous 3-D FDTD solution of Maxwell's equations [18–20]. Our technique accurately synthesizes microscope images of arbitrary inhomogeneous samples under various imaging parameters, incorporating RI fluctuations as fine as 10 nm. We synthesized bright-field, plane-wave epi-illumination microscope images of samples with a RI distribution resembling that of biological cells: $n_1 = 1.53$ [13,14], $n_1 \sigma_{n_\Delta} = 0.05$ [21].

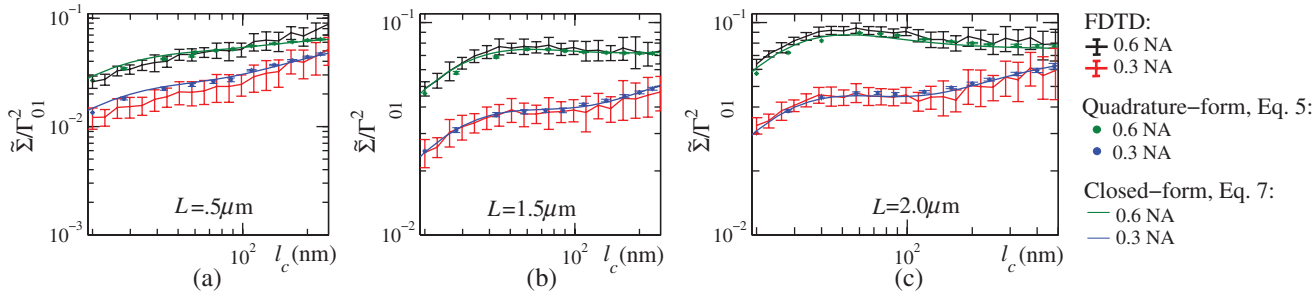

FIG. 3 (color). Illustration of $\tilde{\tilde{\Sigma}}$ dependence on l_c predicted by the quadrature-form [Eq. (5)] and the closed-form [Eq. (7)] analytical expressions for $\tilde{\tilde{\Sigma}}$ (circles and solid lines, respectively) and by FDTD (solid lines with error bars representing standard deviation between 20 realizations of each statistical condition), calculated for (a) $L = 0.5$ μm, $\Delta k = 4.9$ μm^{-1}, $k_c = 16.8$ μm^{-1}, (b) $L = 1.5$ μm, $\Delta k = 4.9$ μm^{-1}, $k_c = 16.8$ μm^{-1}, and (c) $L = 2.0$ μm. $\Delta k = 11.9$ μm^{-1}, $k_c = 18.1$ μm^{-1} (wave number values inside the sample). Data are shown normalized by Γ_{01}^2, the image intensity in the absence of RI fluctuations inside the sample.

The spatial RI correlation was set to be exponential, and the RIs of the top and bottom media were $n_0 = 1$ and $n_2 = 1.53$.

Referring to Fig. 3, the $\tilde{\tilde{\Sigma}}$ predicted by the present theory [either by the quadrature-form Eq. (5) or the closed-form Eq. (7)] exhibits an excellent agreement with the FDTD-simulated experimental results over a wide range of l_c, L, spectral bandwidth, and NA. The agreement is such that the theoretically predicted $\tilde{\tilde{\Sigma}}$ values by both Eqs. (5) and (7) lie within the standard deviation bars of the FDTD results at all points tested. Whereas the present derivation assumes $\Delta k \ll k_c$, in fact, the closed-form analytical solution is robust for Δk that includes the full range of visible wavelengths [Fig. 3(c)]. This match also justifies the employed scalar-wave approximation as well as that the single scattering approximation applies to RI fluctuations typical for fixed biological cells.

We next describe the l_c dependence of $\tilde{\tilde{\Sigma}}$ and compare its key aspects to those of the commonly used scattering parameters: the backscattering (σ_b) and the total scattering (σ_s) cross sections. The value of σ_b manifests a nonmonotonic dependence on l_c, which makes the inverse problem ambiguous [22], whereas σ_s increases steeply $\propto l_c^3$ and thus is relatively insensitive to structural changes at small length scales [23]. In turn, $\tilde{\tilde{\Sigma}}(l_c)$ is distinguished by three important properties illustrated in Fig. 3. First, unlike σ_b, $\tilde{\tilde{\Sigma}}(l_c)$ can be monotonic. This property is apparent for thin samples [$L < 2$ μm, Figs. 3(a) and 3(b)]. For thicker samples, a smaller collection NA can be chosen so that $\tilde{\tilde{\Sigma}}(l_c)$ remains monotonic [e.g., NA = 0.3 in Fig. 3(c)]. Second, as opposed to $\sigma_s(l_c)$, the sensitivity of $\tilde{\tilde{\Sigma}}$ to changes at smaller length scales is not obscured by changes at larger l_c. We note that the functional form of $\tilde{\tilde{\Sigma}}(l_c)$ for $l_c < 1/k_c$ can be roughly approximated as linear [r^2 values of linear regressions for $\tilde{\tilde{\Sigma}}(l_c)$ presented in Fig. 3 range from 0.86 to 0.91]. Finally, $\tilde{\tilde{\Sigma}}$ is independent of l_c for $l_c \gg 1/k_c$, and therefore $\tilde{\tilde{\Sigma}}(l_c)$ exhibits predominant sensitivity to subdiffraction length scales that is only limited by the signal-to-noise ratio (SNR). The larger structures are naturally resolved in the microscope image. In addition, whereas the above mentioned scattering parameters are $\propto \sigma_{n_\Delta}^2$, $\tilde{\tilde{\Sigma}}$ is $\propto \sigma_{n_\Delta}$ (confirmed by FDTD with $r^2 = 0.99$, data not shown), which substantially improves the SNR.

Results of an FDTD-simulated experiment are shown in Fig. 4. As expected, the bright-field microscope images of samples with $l_c = 20$ and 50 nm [Figs. 4(a) and 4(b)] are essentially indistinguishable. However, a drastic difference between the two samples is revealed in the respective $\Sigma(x', y')$ images [Figs. 4(c) and 4(d), where color bar limits match the ordinate range in Fig. 3(c)]. Figures 4(e) and 4(f) illustrate that a smaller amplitude of

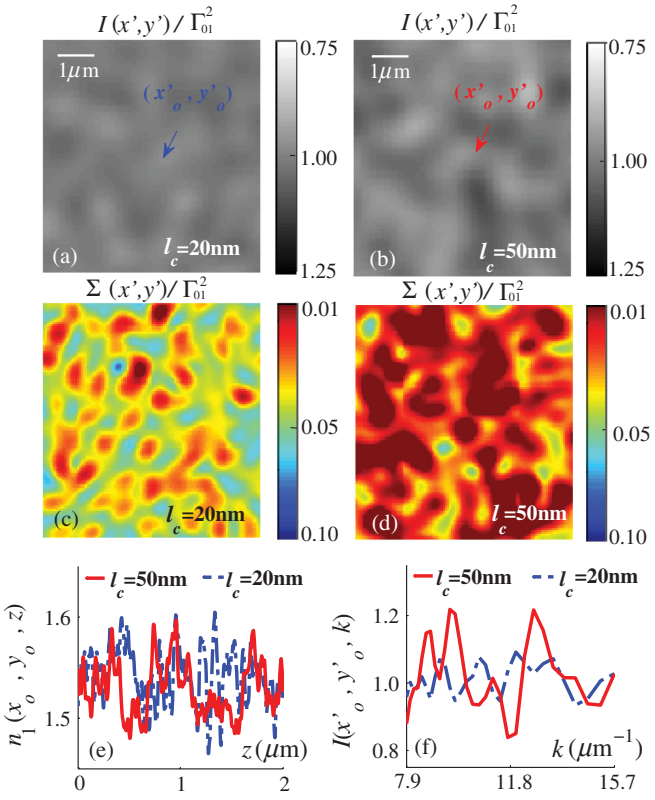

FIG. 4 (color). 40× magnification, 0.6 NA microscope images of samples with $L = 2$ μm were synthesized by FDTD. Bright-field images of samples with (a) $l_c = 20$ nm and (b) $l_c = 50$ nm; $\Sigma(x', y')/\Gamma_{01}^2$ obtained from the wavelength-resolved image of (c) the sample with $l_c = 20$ nm and (d) $l_c = 50$ nm; (e) RI of the two samples as a function of z along central voxels (x_0, y_0), and (f) image spectra of the corresponding pixels (x_0', y_0').

spectral oscillations in the wavelength-resolved microscope image indicates a higher spatial frequency of the sample's RI fluctuations.

Recognizing that the experimental $n_\Delta(\mathbf{r})$ may not be exponentially correlated, one may attempt to (a) use the validated approximations to obtain a closed form solution for a different functional form of the PSD from Eq. (5), (b) represent the correlation function of n_Δ as a superposition of exponentials, or (c) evaluate Eq. (5) numerically (no explicit functional form of the PSD is required for the latter two).

We emphasize that whereas $\tilde{\tilde{\Sigma}}$ does not probe spatial frequencies above $2k$, the subdiffraction-scale structural alterations change the width of PSD and, therefore, the value of $\tilde{\tilde{\Sigma}}$. Thus, $\tilde{\tilde{\Sigma}}$ provides a monotonic *measure* for the width of the 3-D PSD of RI fluctuations with a high sensitivity to subdiffractional length scales, without actually *imaging* the 3-D RI.

We have established that despite the diffraction limit of resolution, the interferometric spectroscopy of scattered

light can quantify the statistics of RI fluctuations at deeply subdiffractional length scales. We have shown that $\tilde{\Sigma}$ obtained from an elastic, label-free, spectrally resolved far-field microscope image quantifies RI fluctuations inside weakly scattering media at length scales limited by the SNR of the detector. We have derived a closed-form analytical solution for $\tilde{\Sigma}$ that yields results that agree with numerical solutions of Maxwell's equations over a wide tested range of sample and instrument parameters. Potential applications include semiconductors, material science, biology, and medical diagnostics.

This work was supported by National Institutes of Health (NIH) Grants No. R01CA128641, No. R01EB003682, and No. R01CA155284 and National Science Foundation (NSF) Grant No. CBET-0937987. The FDTD simulations were made possible by a computational allocation from the Quest high-performance computing facility at Northwestern University.

*Corresponding author.
v-backman@northwestern.edu

[1] D. Lu and Z. Liu, Nat. Commun. **3**, 1205 (2012).
[2] A. Sentenac, P. C. Chaumet, and K. Belkebir, Phys. Rev. Lett. **97**, 243901 (2006).
[3] S. W. Hell, Science **316**, 1153 (2007).
[4] B. Huang, W. Wang, M. Bates, and X. Zhuang, Science **319**, 810 (2008).
[5] D. W. Piston, Trends Cell Biol. **9**, 66 (1999).
[6] G. Popescu, *Quantitative Phase Imaging of Cells and Tissues*, McGraw-Hill Biophotonics (McGraw-Hill, New York, 2011).
[7] Z. Wang, L. Millet, M. Mir, H. Ding, S. Unarunotai, J. Rogers, M. U. Gillette, and G. Popescu, Opt. Express **19**, 1016 (2011).
[8] B. Bhaduri, H. Pham, M. Mir, and G. Popescu, Opt. Lett. **37**, 1094 (2012).
[9] H. Subramanian, P. Pradhan, Y. Liu, I. R. Capoglu, J. D. Rogers, H. K. Roy, R. E. Brand, and V. Backman, Opt. Lett. **34**, 518 (2009).
[10] I. Itzkan, L. Qiu, H. Fang, M. M. Zaman, E. Vitkin, I. C. Ghiran, S. Salahuddin, M. Modell, C. Andersson, L. M. Kimerer, P. B. Cipolloni, K.-H. Lim, S. D. Freedman, I. Bigio, B. P. Sachs, E. B. Hanlon, and L. T. Perelman, Proc. Natl. Acad. Sci. U.S.A. **104**, 17 255 (2007).
[11] S. A. Alexandrov, S. Uttam, R. K. Bista, K. Staton, and Y. Liu, Appl. Phys. Lett. **101**, 033702 (2012).
[12] A. Taflove and S. C. Hagness, *Computational Electrodynamics: The Finite-Difference Time-Domain Method* (Artech House, Norwood, 2005), 3rd ed.
[13] D. Cook, *Cellular Pathology: An Introduction to Techniques and Applications* (Scion, Bloxham, 2006).
[14] G. C. Crossmon, Stain technology **24**, 241 (1949).
[15] M. Born and E. Wolf, *Electromagnetic Theory of Propagation, Interference and Diffraction of Light*, edited by M. Born and E. Wolf (Cambridge University Press, Cambridge, England, 1998).
[16] J. Goodman, *Introduction To Fourier Optics*, McGraw-Hill Physical and Quantum Electronics Series (Roberts & Co., Englewood, 2005), pp. 126–154.
[17] See the Supplemental Material at http://link.aps.org/supplemental/10.1103/PhysRevLett.111.033903 for a detailed derivation.
[18] I. R. Capoglu, ANGORA: A free software package for finite-difference time-domain (FDTD) electromagnetic simulation (2012), date accessed: April 2012, http://www.angorafdtd.org.
[19] I. R. Capoglu, J. D. Rogers, A. Taflove, and V. Backman, in *Progress in Optics*, Vol. 57, edited by E. Wolf (Elsevier, New York, 2012), pp. 1–91.
[20] I. R. Capoglu, A. Taflove, and V. Backman, IEEE Trans. Antennas Propag. (to be published).
[21] J. M. Schmitt and G. Kumar, Appl. Opt. **37**, 2788 (1998).
[22] A. Ishimaru, *Wave Propagation and Scattering in Random Media*, IEEE Press Series on Electromagnetic Wave Theory (Wiley, New York, 1999).
[23] A. J. Radosevich, J. Yi, J. D. Rogers, and V. Backman, Opt. Lett. **37**, 5220 (2012).